

## Tidal Disruptions of Main Sequence Stars - V. The Varieties of Disruptions

JULIAN KROLIK,<sup>1</sup> TSVI PIRAN,<sup>2</sup> AND TAEHO RYU<sup>1</sup>

<sup>1</sup>*Physics and Astronomy Department, Johns Hopkins University, Baltimore, MD 21218, USA*

<sup>2</sup>*Racah Institute of Physics, Hebrew University, Jerusalem 91904, Israel*

(Received; Revised; Accepted)

Submitted to ApJ

### ABSTRACT

Tidal disruption events (TDEs), events in which a star passes very close to a supermassive black hole, are generally imagined as leading either to the star’s complete disruption or to its passage directly into the black hole. In the former case it is widely believed that in all cases the bound portion of the debris quickly “circularizes” due to relativistic apsidal precession, i.e., forms a compact accretion disk, and emits a flare of standardized lightcurve and spectrum. We show here that TDEs are more diverse and can be grouped into several distinct categories on the basis of stellar pericenter distance  $r_p$ ; we calculate the relative frequency of these categories. In particular, because rapid circularization requires  $r_p \lesssim 10r_g$  ( $r_g \equiv GM_{\text{BH}}/c^2$ ), it can happen in only a minority of total disruptions,  $\lesssim 1/4$  when the black hole has mass  $M_{\text{BH}} = 10^6 M_{\odot}$ . For larger pericenter distances,  $10 < r_p/r_g < 27$  (for  $M_{\text{BH}} = 10^6 M_{\odot}$ ), main sequence stars are completely disrupted, but the bound debris orbits are highly eccentric and possess semimajor axes  $\sim 100 \times$  the scale of the expected compact disk. Partial disruptions with fractional mass-loss  $\gtrsim 10\%$  should occur with a rate similar to that of total disruptions; for fractional mass-loss  $\gtrsim 50\%$ , the rate is  $\approx 1/3$  as large. Partial disruptions—which must precede total disruptions when the stars’ angular momenta evolve in the “empty loss-cone” regime—change the orbital energy by factors  $\gtrsim O(1)$ . Remnants of partial disruptions are in general far from thermal equilibrium. Depending on the orbital energy of the remnant and conditions within the stellar cluster surrounding the SMBH, it may return after hundreds or thousands of years and be fully disrupted, or it may rejoin the stellar cluster.

*Keywords:* black hole physics – gravitation – hydrodynamics – galaxies:nuclei – stars: stellar dynamics

### 1. INTRODUCTION

Tidal disruptions of main sequence stars by supermassive black holes were first discussed  $\sim 40$  years ago (Hills 1976; Frank & Rees 1976; Lightman & Shapiro 1977; Lacy et al. 1982), and a characteristic shape for their lightcurves was proposed  $\sim 30$  years ago: a sharp rise to a peak over roughly a month, followed by a decline  $\propto t^{-5/3}$ . This characteristic shape follows from the argument made by Rees (1988) and Phinney (1989) that the bound part of the debris stream returns to the pericenter at a rate  $\propto t^{-5/3}$  supplemented by the assertion

that relativistic apsidal precession rapidly circularizes its orbit; the debris then forms a compact accretion disk whose accretion onto the black hole powers the event.

Several complications can make TDEs more diverse than this picture. Events in which the pericenter distance  $r_p \leq R_{\text{dc}}$  lead to direct capture without tidal disruption;  $R_{\text{dc}} = 4r_g$  ( $r_g \equiv GM/c^2$ ) for non-spinning black holes, and has only a very weak dependence on spin after averaging over orientation (Kesden 2012).

At slightly larger radii, but only when  $r_p$  is less than the radius  $R_{\text{circ}}$ , apsidal precession can be strong enough to perform the role expected of it, driving rapid circularization and compact accretion disk formation. In Schwarzschild spacetime, the apsidal direction of highly-eccentric orbits is rotated by  $\sim (10r_g/r_p)$  radian per pericenter passage, suggesting that  $R_{\text{circ}} \simeq 10r_g$ ; in

Corresponding author: Julian Krolik  
 jhk@jhu.edu

Kerr, orbital plane precession may also diminish the probability of close-in debris stream intersection (Dai et al. 2013; Guillochon & Ramirez-Ruiz 2015).

Because  $\mathcal{R}_t$ , the physical tidal radius within which stars are fully disrupted, can be considerably larger than  $R_{\text{circ}}$  ( $\mathcal{R}_t \simeq 27r_g$  for  $M_* \lesssim 3$  when  $M_{\text{BH}} = 10^6 M_{\odot}$  (Ryu et al. 2019c,a)), for most TDEs in which the star is fully disrupted, quick formation of a compact accretion disk does not necessarily occur. The outcome of these events is then very different from those in which the bound matter quickly finds its way into a compact accretion disk (Piran et al. 2015; Krolík et al. 2016).

At even larger pericenter distances, stars undergo partial disruptions, events in which only a fraction of the star is disrupted, and a significant, but perturbed, remnant remains. These take place when  $\mathcal{R}_t < r_p < \hat{R}_t$ , where we define  $\hat{R}_t$  as the maximum pericenter within which at least a few percent of the star’s mass is lost. The ratio  $\hat{R}_t/\mathcal{R}_t$  varies by factors of a few with  $M_*$  and  $M_{\text{BH}}$ ; it is  $\simeq 2$  for  $M_* = 1$  and  $M_{\text{BH}} = 10^6$  (Ryu et al. 2019b). From here on, all masses will be given in units of the solar mass and all stellar radii in units of the solar radius.

Flares from partial TDEs should differ from those of both varieties of full TDE because the energy distribution of the bound debris is narrow and offset from  $E = 0$ , leading to a mass fallback rate that peaks somewhat later than for full disruptions and declines much more rapidly (Ryu et al. 2019b). In addition, the remnant, which is initially much more extended and rotates much more rapidly than a main sequence star of its mass, can suffer quite disparate fates depending on how quickly it cools and the size of its orbit’s semimajor axis (Ryu et al. 2019b).

Finally, we note that if the SMBH is accreting before the star approaches, even at a slow rate, the interaction of the returning streams with the pre-existing accretion disk adds an entirely different aspect of diversity (Chan et al. 2019). In this case, the most dramatic effect of the encounter is a rapid infall of the inner accretion disk onto the SMBH. The observed light curve then bears no resemblance to the classical  $t^{-5/3}$  shape.

It is the thrust of this paper to expand upon these distinctions based on  $r_p$  and to link (somewhat speculatively) the dynamical contrasts they imply with observational contrasts. In order of their size, which is also the order in which we will discuss them, we call these different regimes: “circularized total disruptions” ( $R_{\text{dc}} < r_p \leq R_{\text{circ}}$ ); “common total disruptions” ( $R_{\text{circ}} < r_p \leq \mathcal{R}_t$ ); “partial disruptions” ( $\mathcal{R}_t < r_p < \hat{R}_t$ ); and “unconventional total disruptions”. The last term refers to a total disruption of a partial disruption

remnant in which the remnant did not have time to relax to a steady state configuration before returning to the black hole. Although the transition between the different regimes is not perfectly sharp, the key properties vary rapidly enough with  $r_p$  to make these distinctions useful.

The structure of the paper is as follows. In §2 we discuss some of the relevant theoretical background and summarize some results from recent numerical simulations. We then turn to discuss different varieties of TDEs in order of increasing pericenter distance beginning with “circularized total disruptions” in §3, continuing with “common total disruptions” in §4, turning to partial disruptions in §5 and concluding in §6 with “unconventional total disruptions”. In each section we discuss first the basic dynamics, then speculate about their distinctive observational signatures, and lastly estimate the relative event rate of the regime in question.

## 2. BACKGROUND

### 2.1. Mass fallback rate and lightcurves

The argument that the bolometric luminosity as a function of time is  $\propto t^{-5/3}$  for times after the peak fallback rate begins with an estimate of the energy distribution in the debris resulting from the disruption: spread symmetrically around zero with a half-width  $\Delta\epsilon \sim GM_{\text{BH}}R_*/r_t^2$ , where  $M_{\text{BH}}$  is the mass of the black hole,  $M_*$  and  $R_*$  are the mass and radius of the unperturbed star, and  $r_t \equiv R_*(M_{\text{BH}}/M_*)^{1/3}$  is an order of magnitude estimate for the distance at which tidal forces are important. The period of orbits with binding energy  $\Delta\epsilon$  is  $t_0 \simeq 0.11M_*^{-1}R_*^{3/2}M_{\text{BH},6}^{1/2}$  yr. This estimate explains the month-timescales. From here on, all masses will be given in units of  $M_{\odot}$ , all stellar radii in units of the Solar radius, and  $M_{\text{BH},6} \equiv M_{\text{BH}}/10^6$ .

Given an angular momentum consistent with an orbit of pericenter  $r_p \sim r_t$  and an orbital energy of the estimated scale, the orbits of the bound debris must be highly eccentric:  $1 - e \leq 2(M_*/M_{\text{BH}})^{1/3} = 0.02M_*^{1/3}M_{\text{BH},6}^{-1/3}$ . The rate at which mass returns to the star’s pericenter immediately follows from a chain rule differentiation once the distribution of mass with energy,  $dM/dE$ , is determined. Rees (1988) argued that  $dM/dE$  should be flat between  $-\Delta\epsilon$  and  $+\Delta\epsilon$ , and detailed calculations employing realistic main-sequence internal density profiles for the stars have confirmed that this is a reasonable zeroth-order approximation (Goicovic et al. 2019; Golightly et al. 2019b; Law-Smith et al. 2019; Ryu et al. 2019a). However, calculations using both general relativity and realistic stellar profiles also show that the energy-spread of the debris  $\Delta E$  can differ from the estimate  $\Delta\epsilon$  by factors  $\sim 2$ : a decrease of this magnitude

for  $M_* \lesssim 0.5$ , an increase of this magnitude for  $M_* \gtrsim 1$  (Ryu et al. 2019a).

To predict the resulting lightcurve requires translating this mass-return rate, derived only from simple orbital mechanics, to a dissipation rate coupled to a photon diffusion rate. In the initial theory, it was supposed that relativistic apsidal precession would create strong shocks within the returning debris. Having dissipated much of the orbital energy into heat, the material would then settle into a hot accretion disk with an outer radius  $\sim 2r_p$ . The time for matter to accrete all the way to the black hole’s innermost stable circular orbit (ISCO) would then be short compared to  $t_0$ , so the luminosity would follow the return rate if the accretion flow is radiatively efficient. In what follows, we will discuss the degree to which this view is upheld by subsequent work.

## 2.2. Characteristic angular momenta

Parabolic stellar orbits can be characterized by a single parameter because their pericenters are functions of angular momentum alone. In Schwarzschild spacetime, the relation between angular momentum and pericenter for a parabolic orbit is

$$L^2(r_p) = 2[(r_p/r_g)^2/(r_p/r_g - 2)](r_g c)^2; \quad (1)$$

spin corrections to this relation are relatively small,  $\sim (a/M)/(L/r_g c)$ .

In addition, as we discuss below, event rates are more directly related to the stellar specific angular momentum  $L_*$  than to the pericenter  $r_p$ . It is therefore convenient to define the angular momenta of orbits with the pericenters separating the relevant TDE categories:  $L_{\text{dc}} \equiv L(R_{\text{dc}})$ ,  $L_{\text{circ}} \equiv L(R_{\text{circ}})$ ,  $\mathcal{L}_t \equiv L(\mathcal{R}_t)$ , and  $L_{\text{partial}} \equiv L(\hat{R}_t)$ .

For orbits in the equatorial plane of a spinning black hole,  $L_{\text{dc}} = 2(1 + \sqrt{1 - a/M})r_g c$ ; averaging over all orbital orientations in Kerr spacetime,  $\langle L_{\text{dc}} \rangle \simeq 4r_g c$  with very small error (Kesden 2012).

If  $R_{\text{circ}} \simeq 10r_g$  as estimated above, it is a reasonable approximation to adopt the Schwarzschild value for  $L_{\text{circ}} = 5r_g c$ . However, the more detailed geometric argument of Dai et al. (2015) suggested that even for  $r_p = 10r_g$ , the stream-intersection shock would dissipate rather less than the orbital energy, thereby creating an eccentric disk whose outer radius is  $\sim 10r_p$ . Because this calculation employed a lowest-order post-Newtonian approximation to calculate the apsidal precession and considered only shock geometry rather than full shock hydrodynamics, this estimate of the resulting disk size carries some intrinsic uncertainty. In the following, we will use  $R_{\text{circ}} = 10r_g$  as a fiducial value, but it is possible that it may be an overestimate.

As previously remarked, Ryu et al. (2019a) found that  $\mathcal{R}_t \simeq 27r_g$ , almost independent of  $M_*$ , when  $M_{\text{BH}} = 10^6$ . Ryu et al. (2019c) showed that, as a function of black hole mass,  $\mathcal{R}_t/r_g \approx 23 + (M_{\text{BH}}/10^6)^{-2/3}$ . The corresponding  $\mathcal{L}_t$  follows from Equation 1.

## 2.3. Rates

The functional relation between event rate and event pericenter depends on how the surrounding stars evolve in angular momentum. Most calculations in the literature (e.g. Stone & Metzger (2016)) assume that the evolution is dominated by gravitational interactions with other stars, but mechanisms such as resonant relaxation (Rauch & Tremaine 1996; Rauch & Ingalls 1998) or triaxiality in the stellar cluster (Merritt 2013) may also operate. No matter which mechanism dominates, if the stars’ orbital dynamics evolve in a fashion such that the change in angular momentum per stellar orbit is large compared to the angular momentum associated with  $r_p = r_t$ , their evolutionary regime is called “full loss-cone” or “pinhole” (Frank & Rees 1976; Lightman & Shapiro 1977). In this regime, the stellar angular momentum distribution is smooth across the range of angular momenta associated with tidal disruption events. The rate of an event with  $r \leq r_p$  is therefore proportional to the solid angle of the loss-cone in angular momentum space, which is  $\propto L^2(r_p)$ .

The rate per black hole of TDEs of a given class in this orbital-evolution regime is

$$S = [L_{\text{max}}^2 - L_{\text{min}}^2] \int dE_* \frac{\partial^2 f}{\partial L_*^2 \partial E_*}(L_* = 0, E_*) P_*^{-1}(E_*), \quad (2)$$

where  $L_{\text{max}}$  and  $L_{\text{min}}$  define the range of angular momentum in which this class of event occurs,  $df/dL_*^2$  is the distribution function of stars in the surrounding cluster with respect to the square of the stellar angular momentum,  $E_*$  is the stellar specific energy, and  $P_*(E_*)$  is the star’s orbital period.

The situation is very different in the empty loss-cone regime, in which the rate of angular momentum evolution is so slow that every time a star passes through apocenter, its squared angular momentum changes by an amount  $\Delta L_*^2 \ll |L(\mathcal{R}_t)|^2$ . In this regime, stars undergo a random walk in angular momentum space until they find themselves with  $L_*^2$  slightly less than  $\mathcal{L}_t^2$ , and are then destroyed by a total disruption. In this limit, the rate of total disruptions is  $\propto \ln \mathcal{L}_t$  (Lightman & Shapiro 1977), augmented at about the 10% level by occasional strong encounters (Weissbein & Sari 2017).

## 3. CIRCULARIZED TOTAL DISRUPTIONS

### 3.1. Structure and radiation

We call a tidal disruption “circularized” if the relativistic apsidal precession of the orbit is large enough ( $\gtrsim 1$  radian) that the apsidal axes of the early-returning debris streams swing around so that they strike the slightly later-returning streams at a large angle. The shock speed is then of order the free-fall speed near  $r_p$ , so that much of the orbital kinetic energy is dissipated into heat. The result is an extremely hot gas, one with internal energy per nucleon  $\langle \epsilon \rangle \simeq 20(R_{\text{circ}}/r_p)(v_s/v_{\text{ff}})^2$  MeV, for shock speed  $v_s$  and free-fall speed  $v_{\text{ff}}$  at the location of the shock. Supported partly by the pressure due to this internal energy and partly by rotation (by definition, the specific angular momentum of the matter is comparable to what is needed for a circular orbit at this radius), the debris should form a geometrically thick disk.

Even if the debris had the density of the original star, at such a high temperature radiation would completely dominate the internal energy, so the immediately post-shock thermodynamic temperature is  $\ll \langle \epsilon \rangle$ ,

$$T \sim (\rho \langle \epsilon \rangle / m_p a_{\text{th}})^{1/4} \quad (3)$$

$$\sim 2 \times 10^7 [\rho_{-4} (R_{\text{circ}}/r_p)]^{1/4} (v_s/v_{\text{ff}})^{1/2} \text{ K},$$

where we have scaled to a debris density  $\sim 10^{-4}$  gm cm $^{-3}$  on the supposition that  $\rho \sim \rho_* R_*/a_0 \sim \rho_* (M_*/M_{\text{BH}})^{2/3}$ , for  $a_0$  the scale of the debris orbits’ semimajor axes and  $a_{\text{th}}$  the Stefan-Boltzmann constant for radiation energy density. Thermal radiation can balance the rate at which debris orbital energy is dissipated, so one might expect a surface temperature determined by their equilibration:

$$T_s \sim 1 \times 10^6 M_*^{0.14} M_{\text{BH},6}^{-5/8} (R_{\text{circ}}/r_p)^{3/4} \quad (4)$$

$$\times (v_s/v_{\text{ff}})^{1/2} (t/t_0)^{-5/12} \text{ K}.$$

The exponent of  $M_*$  comes from an approximation to the main-sequence mass-radius relation  $R_* \propto M_*^{0.88}$  (Ryu et al. 2019a).

The associated luminosity would be

$$L \sim 2 \times 10^{45} M_*^{0.56} M_{\text{BH},6}^{-1/2} (R_{\text{circ}}/r_p) \quad (5)$$

$$\times (v_s/v_{\text{ff}})^2 (t/t_0)^{-5/3} \text{ erg s}^{-1}.$$

This is  $\sim 10L_E$  for  $M_{\text{BH}} \sim 10^6$ , so that  $L/L_E \propto M_{\text{BH}}^{-3/2}$ . Energy derived from accretion can in principle increase this by a factor of order unity, but by no more than that, because this already represents an energy per unit mass  $0.1(R_{\text{circ}}/r_p)c^2$ . As the estimated temperature indicates, it would emerge primarily in the soft X-ray band.

However, both the temperature and the luminosity could also be overestimates. As we have already mentioned, the analysis of Dai et al. (2015) indicated that

when  $r_p \simeq 10r_g$ , only a portion of the orbital energy is dissipated. In addition, it is possible that the accretion time is short compared to the cooling time. This could be the case if the only internal heat transport mechanism is photon diffusion (Begelman 1979). Whether this is so depends on the internal dynamics. If MHD turbulence driven by the magnetorotational instability achieves the amplitude found in ordinary super-Eddington disks, photon diffusion may be supplemented by photons trapped in magnetically-buoyant bubbles (Blaes et al. 2011; Jiang et al. 2014). On the other hand, because the angular momentum in the debris,  $< 5r_g c$  by definition, is only slightly greater than the maximum angular momentum permitting passage through the event horizon for weakly-bound matter ( $4r_g c$ ), comparatively weak internal stresses are required for accretion, so the amplitude of MHD turbulence may be relatively low—which would also limit the additional dissipation associated with accretion.

Super-Eddington luminosity may drive an outflow carrying a sizable fraction of the net accretion rate (Dai et al. 2018; Jiang et al. 2019). If so, it would be optically thick out to a radius  $\gg r_p$ ; as a result, the emerging spectrum would be diminished in energy by a factor  $\sim (r_p/r_{\text{photo}})^{1/2}$  for photospheric radius  $r_{\text{photo}}$  (Strubbe & Quataert 2009; Dai et al. 2018). So far simulations have not been able to make a clear prediction of  $r_{\text{photo}}$  or its dependence on system parameters.

After a few  $t_0$ , nearly all the bound mass will have returned to the black hole and joined the compact disk. From this point on, it is no longer a disk in inflow equilibrium, i.e., one whose mass accretion rate at every radius matches the feeding rate at its outer radius (modulo local fluctuations). Rather, it is a disk that is intrinsically in a state of inflow *disequilibrium* because it continues to accrete onto the black hole even while it no longer receives new mass at the outside (Shen & Matzner 2014). Recent formal models of such a disk employing general relativistic dynamics and permitting non-zero stress at the ISCO (as found in global MHD simulations: Noble et al. (2010); Schnittman et al. (2016); Avara et al. (2016)) lead to a slow decline in the total disk dissipation rate  $\propto t^{-n}$  with  $0.5 \lesssim n \lesssim 1$  (Balbus & Mummery 2018; Mummery & Balbus 2019).

### 3.2. Rate

Equation 2 gives the event rate when stellar evolution results in a full loss-cone. To evaluate it, we need to identify  $L_{\text{min}}$  and  $L_{\text{max}}$ . In this context,  $L_{\text{min}}^2 = L_{\text{dc}}^2 = (4r_g c)^2$ , while  $L_{\text{max}}^2 = \min(L_{\text{circ}}^2, L_{\text{t}}^2)$ . Consequently,  $L_{\text{max}}^2$  can never be more than  $L_{\text{circ}}^2 = 25(r_g c)^2$ ; it immediately follows that  $L_{\text{max}}^2 - L_{\text{min}}^2 \leq 9(r_g c)^2$ , and

the fraction of all events with  $r_p \leq R_{\text{circ}}$  resulting in tidal disruptions rather than direct capture is always  $\leq 0.36$ , *independent of both  $M_*$  and  $M_{\text{BH}}$* .

The situation for empty loss-cone evolution is different. The rate of rapidly-circularizing total disruptions is an even smaller fraction of all total disruptions so long as  $\mathcal{R}_t$  is significantly greater than  $R_{\text{circ}}$ . The only avenue to a rapid circularization event is through the  $\sim 10\%$  probability channel provided by the tail of the stellar scattering angular momentum exchange distribution [Weissbein & Sari \(2017\)](#).

However,  $\mathcal{R}_t \sim R_{\text{circ}}$  when  $M_{\text{BH}} \gtrsim 5 \times 10^6$ , so that the change in angular momentum required to take a star from its last value of  $L$  for a partial disruption to  $\leq L_{\text{circ}}$  might be  $\ll \mathcal{L}_t$ . For these higher-mass black holes, provided  $-\Delta L_* < L_* - L_{\text{dc}}$ , empty loss-cone evolution leads almost exclusively to circularized total disruptions, modulo an exception to be discussed in § 6. Of course, when  $L_* < L_{\text{dc}}$ , even slow angular momentum evolution ultimately leads to capture rather than total disruption.

## 4. COMMON TOTAL DISRUPTIONS

### 4.1. *Structure and radiation*

In this class of events, the star is totally disrupted, but the stellar pericenter is too large for there to be strong apsidal precession. As a result, the apsidal precession causes orbital intersection between debris streams with different return times near their orbital apocenters rather than near their pericenters ([Shiokawa et al. 2015](#)). Because the eccentricity is so large, this means the kinetic energy available for dissipation is much smaller than if the intersection took place near pericenter, typically by a factor  $\sim 100$ . This fact substantially alters the evolution of debris orbits, with most of the bound debris mass entering an asymmetric, highly elliptical flow. Two new shocks appear within this flow, also in the apocenter region, with strengths comparable to the stream intersection shock ([Shiokawa et al. 2015](#)). Over a time  $\simeq 10t_0$ , these shocks gradually diminish in magnitude as the mass-return diminishes.

When they no longer act, the only mechanism capable of transferring angular momentum is MHD turbulence stirred by the magnetorotational instability. Its linear growth rate in these circumstances is comparable to that found in circular orbits ([Chan et al. 2019](#)); if its growth to nonlinear saturation takes  $\sim 10$  orbits, as is the case for circular orbit flows, it does not begin until  $\sim 10t_0$  after the disruption, and even when it does, the accretion time from these larger radii is likely to be a multiple of the orbital time, i.e.,  $\gg t_0$ . Accretion of the majority of the bound mass may therefore be a relatively slow process.

On the other hand, a non-negligible minority is deflected by the “nozzle shock” that forms where the streams converge toward the orbital plane as they approach  $r \sim r_p$ . This portion of the debris actually can enter a compact accretion disk ([Shiokawa et al. 2015](#)). However, this does not necessarily happen on the gas’s first passage through pericenter; the entire process may require up to  $\simeq 10t_0$  to go to completion ([Shiokawa et al. 2015](#)).

Such a dynamical situation has several implications regarding observable properties. The apocenter-region shocks have total heating rates quite similar to the observed optical/UV luminosity ( $\sim 10^{44} \text{ erg s}^{-1}$ ) over the period  $\simeq 3 - 10t_0$  after the star’s pericenter passage; the warmed area is also similar ([Piran et al. 2015; Krolik et al. 2016](#)) to the size inferred from the temperature ( $\sim 2 - 4 \times 10^4 \text{ K}$ ) of the thermal spectrum seen in that band (e.g., the large sample reported in [van Velzen et al. \(2020\)](#)). The orbital speeds in that region are likewise similar to the observed widths of emission lines.

Accretion through the compact disk produces a similar luminosity for about the same time, and with an effective temperature ([Krolik et al. 2016](#)) not far from the  $\simeq 50 - 100 \text{ eV}$  commonly seen ([van Velzen et al. 2020](#)). When the slowly accreting matter coming in from the apocenter region begins to arrive, one might expect a slow decay in the disk luminosity as well as a slow decrease in its characteristic temperature.

### 4.2. *Rate*

Once again, the rate of full loss-cone events is given by Equation 2, but  $L_{\text{max}}^2 = \mathcal{L}_t^2$  and  $L_{\text{min}}^2 = L_{\text{circ}}^2$ . For  $M_{\text{BH}} = 10^6$ , the nearly  $M_*$ -independent value of  $\mathcal{R}_t$  is  $\simeq 27r_g$  ([Ryu et al. 2019c,a](#)); this translates to  $\mathcal{L}_t^2 = 58(r_g c)^2$ , so that  $\mathcal{L}_t^2 - L_{\text{circ}}^2 = 33(r_g c)^2$ . Recalling the rate we estimated for circularized total disruptions in the previous section, we see that, for  $M_{\text{BH}} = 10^6$ , the rate of common total disruptions is, for full loss-cone evolution,  $\gtrsim 4 \times$  the rate of rapidly-circularizing total tidal disruptions.

The rate of common total disruptions due to empty loss-cone evolution is the classical rate  $\propto \ln \mathcal{L}_t$ —but with a complication. To reach the edge of the loss-cone by this means, stars have no choice but to pass through the range of  $L_*^2$  in which partial disruptions take place. Consequently, they *must* lose mass as their angular momentum wanders through this region of phase space, and the fraction of the star’s mass that is lost increases as its angular momentum nears  $\mathcal{L}_t$ . As we will discuss at greater length in § 5, total disruptions reached in this way predominantly involve low-mass stars because even stars beginning the process with high-mass become low-

mass by the time they are completely disrupted. Further complications regarding orbital energy evolution and the thermal state of partial disruption remnants will also be discussed in § 5.

## 5. PARTIAL DISRUPTIONS

### 5.1. Structure and radiation

Like full disruption events, partial disruptions also produce a significant amount of debris, roughly half of which is bound and half unbound, even if the total mass in debris is, by definition, less than in a complete disruption. However, unlike complete disruptions, the energy distribution of the debris is generically bimodal, rather than approximately flat (Goicovic et al. 2019; Ryu et al. 2019b). To the degree that less than all the star’s mass is lost, there is always a depression in  $dM/dE$  for  $E \approx 0$ . This depression is deeper and wider for events with less mass-loss. The immediate consequence is that the mass-return rate for partial disruptions declines more steeply after reaching its peak. For cases in which the star’s mass is reduced by a factor order unity, the post-peak fallback rate is  $\propto t^{-n}$  with  $2 < n < 2.7$ , where, for the same fractional mass-loss,  $n$  is smaller for low-mass stars than for high-mass stars, i.e.,  $M_* \gtrsim 1$  (Ryu et al. 2019b). When  $\lesssim 10\%$  of the star’s mass is lost, the decline steepens substantially, to  $n \simeq 5$  for high-mass stars and  $\simeq 6$  for low-mass stars. In addition, the energy at which  $dM/dE$  peaks is also somewhat smaller in absolute magnitude than the characteristic energy spread for full disruptions (Ryu et al. 2019b). It therefore takes longer for the debris stream to return to the SMBH vicinity, so that the peak mass return rate is reached somewhat later. The magnitude of the mass return rate is also depressed, both because the return is slower and because there is less debris mass than in a full disruption.

Partial disruptions also differ from total disruptions in that they rapidly circularize *only* if  $M_{\text{BH}} \gtrsim 1 \times 10^7$ . Thus, their phenomenology should resemble that of common total disruptions, except for the adjustments to their mass return rate described in the previous paragraph.

### 5.2. Rate

As shown by Ryu et al. (2019c,d), the relation between the fractional remnant mass left after a partial disruption of a main sequence star and the character of the star’s original orbit is a nearly universal function, independent of  $M_*$  and  $M_{\text{BH}}$ , when phrased in terms of the angular momentum of the orbit. To be specific, if we define the variable

$$x_L \equiv \frac{L_*^2 - L_{\text{dc}}^2}{\mathcal{L}_t^2 - L_{\text{dc}}^2}, \quad (6)$$

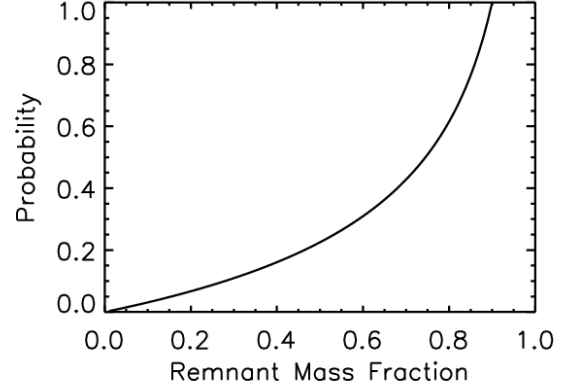


**Figure 1.** The probability that a partial disruption event yields remnant mass fraction  $\leq M_{\text{rem}}/M_*$  as predicted by the relationship between orbital angular momentum and  $M_{\text{rem}}/M_*$  developed in Paper 1.

then

$$\frac{M_{\text{rem}}}{M_*} = 1 - x_L^{-3}. \quad (7)$$

The remnant left behind is within a few percent of the mass of the original star when  $x_L > 3$ .

These relations can be rearranged into the form

$$L_{\text{rem}}^2 = L_{\text{dc}}^2 + \frac{\mathcal{L}_t^2 - L_{\text{dc}}^2}{(1 - M_{\text{rem}}/M_*)^{1/3}}. \quad (8)$$

Once again using the full loss-cone formalism of Equation 2, the rate of events in which the remnant mass fraction is non-zero but  $\leq M_{\text{rem}}/M_*$  is then proportional to  $L_{\text{rem}}^2 - \mathcal{L}_t^2$ . This rate rises very steeply as a function of  $M_{\text{rem}}/M_*$ . For  $M_{\text{BH}} = 10^6$ ,  $(L_{\text{rem}}^2 - \mathcal{L}_t^2)/(r_g c)^2 \simeq 1.5$  for  $M_{\text{rem}}/M_* = 0.1$ , but rises to  $\simeq 11$  for  $M_{\text{rem}}/M_* = 0.5$ ,  $\simeq 25$  for  $M_{\text{rem}}/M_* = 0.75$ , and  $\simeq 50$  for  $M_{\text{rem}}/M_* = 0.9$  (see Fig. 1).

If stars evolve in the full loss-cone regime and  $M_{\text{BH}} = 10^6$ , the rate of events with mass-loss  $\geq 20\%$  is about the same as the rate of common total disruptions; the rate for events with a mass-loss fraction  $\geq 10\%$  is  $\simeq 1.5 \times$  larger. Because empty loss-cone evolution begins to depress the distribution function even for  $L_* > \mathcal{L}_t$ , the rate of events as a function of fractional mass-loss could have an even steeper dependence on  $M_{\text{rem}}/M_*$  than the curve shown in Figure 1. The fact that the probability for an event with a certain fractional mass-loss rises so sharply with decreasing mass-loss means that stars suffer many minor partial disruptions for every major one. The most probable mass-loss history for a star evolving in this regime is therefore to lose most of its mass in a large number of weak events. By the time such a star reaches the threshold for a total disruption, its mass

will, in most instances, be a fairly small fraction of its original mass.

Partial disruptions do not only affect stellar mass: they also change the remnant’s specific orbital energy. In this way, they can also be viewed as accelerating energy evolution, and by that means, possibly even moving stars from one angular momentum evolution regime to the other. In the sample of events examined by Ryu et al. (2019b), the change in energy due to the disruption is comparable to or larger than the typical kinetic energy of bulge stars. When the star’s incoming orbit is one that places it in the full loss-cone regime, its change in angular momentum per orbit  $|\Delta L|$ , although large compared to the tiny loss-cone angular momentum, could nonetheless still be small compared to the circular-orbit angular momentum  $L_0$  corresponding to its energy. Stellar interactions during a single orbit would then change its energy by a fractional amount comparable to  $\max(|L_*|, |\Delta L|)|\Delta L|/L_0^2$ . By contrast, the partial disruption itself changes its energy by a factor of order unity or even greater, significantly accelerating energy evolution. The conventional assumption of tidal disruption rate calculations that energy changes relatively slowly (e.g., as in Stone & Metzger (2016)) is therefore upended. Because the contrast between empty and full loss-cone evolution is largely a matter of energy—higher energy orbits go out farther into the galaxy and have longer orbital periods, both promoting more interaction with other stars—stars can, as a result of a partial disruption, move from empty loss-cone evolution to full loss-cone evolution or vice versa in a single orbit.

Rapid energy evolution is especially important to stars on orbits placing them in the empty loss-cone regime because they *must* suffer partial disruptions before being totally disrupted. Evolution in this regime must therefore account for rapid energy evolution: it is unavoidable.

## 6. UNCONVENTIONAL TOTAL DISRUPTIONS

### 6.1. *Structure and radiation*

In our discussion of the results of partial disruptions up to this point, we have implicitly restricted our analysis to the case in which the stellar remnant is able to relax thermally in less than a single orbital period, so that its structure has reverted to main-sequence by the time of its next pericenter passage. That is not necessarily the case. In the examples studied by Ryu et al. (2019b), the range of orbital periods for bound stars was from  $\sim 400 - 40,000$  yr; for the shorter period stars, even though the excess heat given the remnant is concentrated in its outer layers, there might well not be time to relax thermally before returning to the

black hole. It is important to note in this regard that Ryu et al. (2019b) found short orbital period remnants across the whole range of  $r_p$  values yielding partial disruptions. Because the heating extends deeper inside the remnant when there has been a circularized disruption, their post-disruption structures are more extended, and their cooling times are longer. They are also spun up more strongly.

If a star does encounter the black hole for a second time while in a heated state, it will do so with essentially the same pericenter as before because it is exactly those stars with the shorter orbital periods that are least likely to suffer significant angular momentum change while traveling around an orbit. When it does, it will have a core/halo structure: its core density may be several to tens of times smaller than that of the same-mass main sequence star, but it has an extended envelope whose density falls to much lower values and stretches out to several times the radius of the matched-mass main sequence star. In addition, it can be spun up to a few tens of percent of break-up, especially in the case of severe mass-loss.

The semi-analytic model presented in Ryu et al. (2019c) may provide some rough guidance to the fate of such a star. This model, which reproduces the results of simulations reasonably accurately, predicts that the distance within which a black hole is capable of pulling off matter of a given density is  $\propto \rho^{-1/3}$ . Thus, the primary criterion for a full disruption upon return is that the central density be reduced by a large enough factor (as compared to the original star) that the original pericenter, which produced only a partial disruption, is now within the physical tidal radius of the remnant. Applying this criterion to the remnant sample of Ryu et al. (2019b), it appears that when a star has lost  $\gtrsim 50\%$  of its mass, it will suffer a total disruption upon return if it returns before it relaxes to a more compact configuration. It is plausible that this criterion might be loosened somewhat when, in addition, the remnant’s rapid prograde rotation is taken into consideration; unfortunately, although there exist calculations of the debris energy distribution when such a star is totally disrupted (Golightly et al. 2019a; Kagaya et al. 2019), the degree to which the physical tidal radius is altered has yet to be determined. For those remnants with  $M_{\text{rem}}/M_* \gtrsim 0.5$ , another partial disruption is more likely, but the mass-loss resulting from should be considerably greater than if a main-sequence star of that mass passed at the same distance from the black hole.

The resulting flare from either a total or a partial disruption of such a distended remnant might have noticeably different properties from events due to tides exerted

on a main sequence star. The core/envelope configuration of an uncooled remnant is likely to lead to a rather different energy distribution for the debris mass, perhaps with both a greater concentration toward  $E \approx 0$  and a larger spread in energy. The energy spread could be further enhanced by prograde rotation (Golightly et al. 2019a; Kagaya et al. 2019). As a result, for both full and partial disruptions, the mass-return rate would exhibit an earlier rise and a more gradual decline at late times. Moreover, because the pericenter distances at which these occur are in the range producing exclusively partial disruptions of main sequence stars, their debris can circularize rapidly only if the black hole is extremely massive.

### 6.2. Rate

The rate of unconventional total disruptions depends on how the remnant's orbital period ( $\sim 10^2 - 10^5$  yr as found by Ryu et al. (2019b)) compares to two other timescales: the remnant's thermal relaxation time and the time for dynamical interactions to alter the remnant's angular momentum by more than  $\sim \mathcal{L}_t$ . If the orbital period is shorter than both, the remnant returns to the vicinity of the SMBH with essentially the same pericenter as before, but in a distended state. Preliminary estimates based on the semi-analytic model of Ryu et al. (2019c) show that for  $M_{\text{rem}}/M_* \lesssim 1/2$ , the remnant is sufficiently distended to suffer an unconventional total disruption. Thus, greater mass-loss and shorter orbital periods (the latter for two reasons) favor unconventional disruptions at the next pericenter passage.

Clearly, the rate of these events is most sensitive to the orbital period distribution of remnants and how, if at all, it is correlated with  $M_{\text{rem}}/M_*$ . The rate can be bracketed from above by the rate of partial disruptions (there is at most one such event per partial disruption). For the shorter orbital periods, the lower bound on the rate may be not much smaller. For the longer orbital period portion of the distribution, the lower bound could be much smaller. A detailed quantitative estimate of the rate will require detailed calculations of both the remnant thermal relaxation time and of the distribution of specific orbital energy with which remnants are ejected after a partial disruption.

## 7. DISCUSSION AND SUMMARY

We have distinguished several different regimes of tidal disruption events according to their outcome. The parameter with the greatest influence is the orbital pericenter or, equivalently and more physically informative, the star's orbital angular momentum. The angular momentum has such central interest because it is the quantity most closely related to the rates of the different events.

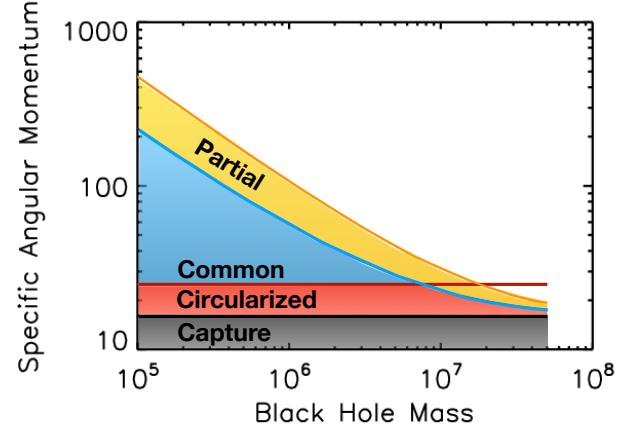


**Figure 2.** Four critical values of  $[L/(r_g c)]^2$ :  $(L_{\text{dc}}/r_g c)^2$  (black line),  $(L_{\text{circ}}/r_g c)^2$  (red line),  $\mathcal{L}_t^2$  (blue curve), and  $\mathcal{L}_{\text{partial}}^2$  defined for  $M_{\text{rem}}/M_* = 0.9$  (orange curve). Direct captures occur for angular momentum in the gray-shaded area below the black line. Circularized total disruptions are found in the red-shaded area. Common disruptions occupy the blue-shaded area. Partial disruptions with  $\geq 10\%$  mass-loss are found in the yellow-shaded area.

In Figure 2, common total disruptions occupy the area between the red and blue curves; circularized total disruptions are found between the red and black lines, or between the blue and black lines when the blue line lies below the red line; direct captures occur for angular momentum below that shown by the black line. Partial disruptions with  $\geq 10\%$  mass-loss are found between the orange and blue curves. As this figure shows clearly, for small black hole mass, only a small fraction of phase space is devoted to circularized total disruptions. At higher black hole mass,  $M_{\text{BH}} \gtrsim 5 \times 10^6$ , all total disruptions are circularized disruptions, but as the black hole mass rises further, they increasingly lose out in competition with direct capture. For most of the relevant black hole mass range, partial disruptions (with mass-loss at least 10%) should take place at a rate similar to that of common total disruptions. By contrast, for the more common black holes with  $M_{\text{BH}} < 5 \times 10^6$ , circularized total disruptions (the rapidly-circularizing variety) are a fraction of the total. For  $M_{\text{BH}} \gtrsim 1 \times 10^7$ , all total disruptions are rapidly-circularizing, but they are also fewer overall because direct capture is already the fate of most events with  $r_p \leq \mathcal{R}_t$ . As can be clearly seen in Figure 2, the Hills mass, the mass above which there is only direct capture, is  $\approx 5 \times 10^7$ .

These different varieties of tidal disruption should be identifiable through their differing observational properties. Common total disruptions should produce thermal optical/UV emission at a temperature  $\sim 2 - 4 \times 10^4$  K, possibly accompanied by thermal X-rays with  $kT \sim$

50 – 100 eV. Their optical/UV lightcurves should show a rise to an approximate plateau, but decline roughly  $\propto t^{-5/3}$  after  $t \approx 10t_0$ . At still later times, the luminosity will depend on how rapidly matter can accrete from the debris apocenter region at  $\sim 10^3 r_g$  to the ISCO region. It is possible that the lightcurve at times  $\gg t_0$  could be relatively shallow, with most of the light not emerging until long after the initial flare peak. This last prediction may explain how it is that in a number of cases, both the UV and X-ray energy radiated 5–10 yr after TDE discovery was about the same as that seen in the first few months (van Velzen et al. 2019; Jonker et al. 2019).

Partial disruptions should resemble common total disruptions in terms of the initially radiated spectrum because the characteristic energy of the debris is, to within factors of 2, about the same. However, because the mass-return rate falls off so much more steeply, the initial plateau is likely to be shorter, and the decline following its end steeper, than in common total disruptions. Like the common total disruptions, partial disruptions may also lead to an extended period of slowly-declining low luminosity emission.

Circularized total disruptions are comparatively rare and could be different. Their intrinsic emission should come at somewhat higher X-ray energies, and these events can produce substantial optical/UV luminosity only by reprocessing. In addition, however, their significantly super-Eddington accretion rates may create qualitatively new phenomena, perhaps explaining the small number of jetted TDEs (Burrows et al. 2011; Bloom et al. 2011; Cenko et al. 2012).

The high mass accretion rate in a circularized disruption event (or in a TDE occurring where there is a pre-existing disk: Chan et al. (2019)) can form a geometrically thick accretion disk. Coughlin & Begelman (2014) suggested that such a disk could drive a relativistic jet by radiation pressure alone. Alternatively, given enough

time, MHD turbulence could build up the magnetic field in the disk until its energy density per unit mass approaches the virial energy of the fluid. Such a field can support a jet whose efficiency in Poynting radiation is  $\sim O(1)$  in terms of accreted rest-mass when the black hole spins rapidly. McKinney et al. (2012), for example, reported that in a disk whose initial field was toroidal, as would likely be the case for disks created by tidal disruptions, there were transient episodes of strong jets. These might be enhanced by the fact that the orbital axes of TDE disks are in general oblique to the spin axis of the black hole, causing field toroidal with respect to the disk to have a poloidal component with respect to the black hole spin.

Unconventional total tidal disruptions will have spectra similar to common total disruptions in virtually every instance. To the degree that their luminosity is tied to mass fallback rate, they may also have broader peaks and slower declines.

We have also shown that partial disruptions can alter the orbital evolution and induce mass evolution of the stars involved. In particular, they drive evolution of orbital energy much faster than gravitational encounters with other stars. This can, in turn, change the pace of the stars’ angular momentum evolution. The induced mass evolution results in eliminating high-mass stars from the population that is ultimately totally disrupted when their angular momentum evolves slowly. Because partial disruptions temporarily distend the remaining star by heating its outer layers, an unconventional total disruption may take place only a single orbit after a severe partial disruption.

## ACKNOWLEDGEMENTS

This work was partially supported by NSF grant AST-1715032 and an advanced ERC grant TReX.

## REFERENCES

Avara, M. J., McKinney, J. C., & Reynolds, C. S. 2016, M.N.R.A.S., 462, 636

Balbus, S. A., & Mummery, A. 2018, M.N.R.A.S., 481, 3348

Begelman, M. C. 1979, M.N.R.A.S., 187, 237

Blaes, O., Krolik, J. H., Hirose, S., & Shabaltas, N. 2011, ApJ, 733, 110

Bloom, J. S., Giannios, D., Metzger, B. D., et al. 2011, Science, 333, 203

Burrows, D. N., Kennea, J. A., Ghisellini, G., et al. 2011, Nat., 476, 421

Cenko, S. B., Krimm, H. A., Horesh, A., et al. 2012, ApJ, 753, 77

Chan, C.-H., Piran, T., Krolik, J. H., & Saban, D. 2019, ApJ, 881, 113

Coughlin, E. R., & Begelman, M. C. 2014, ApJ, 781, 82

Dai, L., Escala, A., & Coppi, P. 2013, ApJL, 775, L9

Dai, L., McKinney, J. C., & Miller, M. C. 2015, ApJL, 812, L39

Dai, L., McKinney, J. C., Roth, N., Ramirez-Ruiz, E., & Miller, M. C. 2018, ApJL, 859, L20

Frank, J., & Rees, M. J. 1976, M.N.R.A.S., 176, 633

Goicovic, F. G., Springel, V., Ohlmann, S. T., & Pakmor, R. 2019, arXiv e-prints, arXiv:1902.08202

Golightly, E. C. A., Coughlin, E. R., & Nixon, C. J. 2019a, *ApJ*, 872, 163

Golightly, E. C. A., Nixon, C. J., & Coughlin, E. R. 2019b, arXiv e-prints, arXiv:1907.05895

Guillochon, J., & Ramirez-Ruiz, E. 2015, *ApJ*, 809, 166

Hills, J. G. 1976, *ApL*, 17, 95

Jiang, Y.-F., Stone, J. M., & Davis, S. W. 2014, *ApJ*, 796, 106

—. 2019, *ApJ*, 880, 67

Jonker, P. G., Stone, N. C., Generozov, A., van Velzen, S., & Metzger, B. 2019, arXiv e-prints, arXiv:1906.12236

Kagaya, K., Yoshida, S., & Tanikawa, A. 2019, arXiv e-prints, arXiv:1901.05644

Kesden, M. 2012, *prd*, 85, 024037

Krolik, J., Piran, T., Svirski, G., & Cheng, R. M. 2016, *ApJ*, 827, 127

Lacy, J. H., Townes, C. H., & Hollenbach, D. J. 1982, *ApJ*, 262, 120

Law-Smith, J., Guillochon, J., & Ramirez-Ruiz, E. 2019, *ApJL*, 882, L25

Lightman, A. P., & Shapiro, S. L. 1977, *ApJ*, 211, 244

McKinney, J. C., Tchekhovskoy, A., & Blandford, R. D. 2012, *M.N.R.A.S.*, 423, 3083

Merritt, D. 2013, *Dynamics and Evolution of Galactic Nuclei*

Mummery, A., & Balbus, S. A. 2019, *M.N.R.A.S.*, 489, 143

Noble, S. C., Krolik, J. H., & Hawley, J. F. 2010, *ApJ*, 711, 959

Phinney, E. S. 1989, in *IAU Symposium*, Vol. 136, The Center of the Galaxy, ed. M. Morris, 543

Piran, T., Svirski, G., Krolik, J., Cheng, R. M., & Shiokawa, H. 2015, *ApJ*, 806, 164

Rauch, K. P., & Ingalls, B. 1998, *M.N.R.A.S.*, 299, 1231

Rauch, K. P., & Tremaine, S. 1996, *NewA*, 1, 149

Rees, M. J. 1988, *Nat.*, 333, 523

Ryu, T., Krolik, J., Piran, T., & Noble, S. 2019a, arXiv e-prints, arXiv:1907.11883

Ryu, T., Krolik, J., Piran, T., & Noble, S. C. 2019b, arXiv e-prints, arXiv:1909.04041

Ryu, T., Krolik, J. H., & Piran, T. 2019c

—. 2019d

Schnittman, J. D., Krolik, J. H., & Noble, S. C. 2016, *ApJ*, 819, 48

Shen, R.-F., & Matzner, C. D. 2014, *ApJ*, 784, 87

Shiokawa, H., Krolik, J. H., Cheng, R. M., Piran, T., & Noble, S. C. 2015, *ApJ*, 804, 85

Stone, N. C., & Metzger, B. D. 2016, *M.N.R.A.S.*, 455, 859

Strubbe, L. E., & Quataert, E. 2009, *M.N.R.A.S.*, 400, 2070

van Velzen, S., Stone, N. C., Metzger, B. D., et al. 2019, *ApJ*, 878, 82

van Velzen, S., Gezari, S., Hammerstein, E., et al. 2020, arXiv e-prints, arXiv:2001.01409

Weissbein, A., & Sari, R. 2017, *M.N.R.A.S.*, 468, 1760